Available online at www.sciencedirect.com
SCIENCE DIRECT®
Journal of Solid State Chemistry 177 (2004) 3448–3453
JOURNAL OF SOLID STATE CHEMISTRY
http://elsevier.com/locate/jssc

Synthesis and optical absorption property of the $Zn_2Ti_xSn_{1-x}O_4$ $(0 \leqslant x \leqslant 1)$ solid solutions

Cun Wang* and Bo-Qing Xu*

Innovative Catalysis Program, Key Lab of Organic Optoelectronics & Molecular Engineering, Department of Chemistry, Tsinghua University, Beijing 100084, China

Received 1 March 2004; received in revised form 6 May 2004; accepted 13 May 2004

Available online 20 July 2004

Abstract

$Zn_2Ti_xSn_{1-x}O_4$ $(0 \leqslant x \leqslant 1)$ solid solutions with an inverse spinel structure (*Fd*3*m*) were synthesized by solid-state reactions at 1300°C of the stoichiometric mixtures of ZnO, TiO_2 and SnO_2. X-ray diffraction, thermogravimetric and differential thermal analyses, scanning electron microscopy, transmission electron microscopy and BET specific surface area measurements were used to gain insights into the solid-state reactions and phase transformation of the system. Optical absorption property of the $Zn_2Ti_xSn_{1-x}O_4$ $(0 \leqslant x \leqslant 1)$ solid solutions was studied with the ultraviolet-visible diffuse reflectance spectroscopy (UV–Vis DRS). The $Zn_2Ti_xSn_{1-x}O_4$ $(0 \leqslant x \leqslant 1)$ solid solutions showed optical absorptions of the semiconductors in the near ultraviolet region; the adsorption band shifts with the composition of the solid solution.

Keywords: Oxides; Chemical synthesis; Crystal structure; Semiconductor; Optical property

1. Introduction

In the past several decades, special attentions have been paid to the systems of many binary oxides such as TiO_2–SnO_2 [1–5], ZnO–TiO_2 [6–10] and ZnO–SnO_2 [11–14] due to their expected wide range of applications. The TiO_2–SnO_2 system was prepared as powders and thin films with various preparations including the sol–gel [4], coprecipitation [15], solid-state reaction [15] and radio frequency sputtering techniques [15]. TiO_2 and SnO_2 in the TiO_2–SnO_2 system will react with each other at high temperatures to form $Ti_xSn_{1-x}O_2$ $(0 \leqslant x \leqslant 1)$ solid solutions with a rutile structure [1,4,15–18]. The TiO_2–SnO_2 system was reported to have applications as photocatalysts [3,17] and gas-sensing materials [2,15,18].

For the ZnO–TiO_2 system, a number of studies have been devoted to the preparation, compound formation and crystal structure, stability, and optical and electrical properties up to now. Calcination of the ZnO–TiO_2 system can lead to three different phases: $ZnTiO_3$ (hexagonal), $Zn_2Ti_3O_8$ (cubic) and Zn_2TiO_4 (cubic) [6–9,19,20], but the formation temperature for each of the $ZnTiO_3$, $Zn_2Ti_3O_8$ and Zn_2TiO_4 phases was shown to vary significantly with the preparation method and the Zn/Ti molar ratio of the starting materials [6–9,19,20]. Both $ZnTiO_3$ and Zn_2TiO_4 phases were found to have important electrical and chemical properties, such as microwave dielectric and catalytic properties [21–23].

For the ZnO–SnO_2 system, the ZnO and SnO_2 components in the system can react with each other to form a stable $ZnSnO_3$ or Zn_2SnO_4 phase, depending on the preparation method and the final calcination temperature [24–27]. The $ZnSnO_3$ phase has been found to show optical, electrical and gas-sensing properties and can be used as optoelectrical [28], gas-sensing [26,29] and lithium ion battery materials [30]. Similar optical [31], electrical [32] and gas-sensing properties [33] were also found for the Zn_2SnO_4 phase.

In this work, polycrystalline powders of $Zn_2Ti_xSn_{1-x}O_4$ $(0 \leqslant x \leqslant 1)$ solid solutions have been synthesized with the solid-state reaction method. And, the powders are characterized with X-ray diffraction

*Corresponding author. Fax: +8610-62792122.
E-mail addresses: wangcun@mail.tsinghua.edu.cn (C. Wang), bqxu@mail.tsinghua.edu.cn (B.-Q. Xu).

0022-4596/$ - see front matter © 2004 Elsevier Inc. All rights reserved.
doi:10.1016/j.jssc.2004.05.024

(XRD), thermogravimetric and differential thermal analyses (TG-DTA), scanning electron microscopy (SEM), transmission electron microscopy (TEM) and specific surface area measurements. We have also studied the optical absorption property of the as-prepared $Zn_2Ti_xSn_{1-x}O_4$ ($0 \leqslant x \leqslant 1$) solid solutions with ultraviolet–visible diffuse reflectance spectroscopy (UV–Vis DRS).

2. Experimental

2.1. Solid state synthesis of the materials

ZnO (zincite, >99.9 wt%, particle size $\sim 0.5\,\mu m$ and BET surface area $\sim 3.3\,m^2/g$), TiO_2 (anatase, >99.8 wt%, particle size ~ 200 nm and BET surface area $\sim 11.4\,m^2/g$) and SnO_2 (cassiterite, >99.9 wt%, particle size ~ 250 nm and BET surface area $\sim 10.5\,m^2/g$) were used as the starting materials. These materials were purchased from Beijing chemical factory of China. Dry mixtures of the ZnO, TiO_2 and SnO_2 at $ZnO/TiO_2/SnO_2$ molar ratios of 2:0:1, 2:0.1:0.9, 2:0.3:0.7, 2:0.5:0.5, 2:0.7:0.3, 2:0.9:0.1 and 2:1:0 were ground in an agate mortar. The mixtures were then calcined in static air at 500°C, 600°C, 700°C, 800°C, 900°C, 1000°C, 1100°C, 1200°C and 1300°C, respectively, for a certain period of time to induce possible solid-state reactions. The products thus obtained were ground in an agate mortar to prepare the powder samples.

2.2. Characterizations of the materials

The XRD analysis was carried out at room temperature with a Bruker D8 Advance diffractometer using Cu$K\alpha$ radiation ($\lambda = 1.5406$ Å). The accelerating voltage, emission current, and scanning speed were 40 kV, 40 mA and 6°/min, respectively. TG-DTA measurements were made on a Setaram TGA/DTA92 thermal analyzer in air. SEM observations were performed with a KYKY2000 microscope (made by the instrumental factory of the Chinese Academy of Sciences) operated at 25 kV. TEM observations were performed with a Hitachi H-800 transmission electron microscope operated at 150 kV. BET surface area measurements were performed on a Micromeritics 2010 instrument.

2.3. Optical absorption study

UV–Vis diffuse reflectance spectra were measured to study the optical absorption property of the samples. The spectra were recorded in air at room temperature with a Hitachi U-3010 spectrophotometer. Pure $BaSO_4$ pellet (Hitachi) was used as the reference sample in all the measurements.

3. Results and discussion

3.1. XRD and crystal phase

Fig. 1(a) and (b) show the X-ray diffraction patterns of the $ZnO/TiO_2/SnO_2$ powders. The $ZnO/TiO_2/SnO_2$ mixture with a Zn/Ti/Sn molar ratio of 4:1:1 was used as a representative to show the solid-state reaction processes of the $ZnO/TiO_2/SnO_2$ mixtures. The results of Fig. 1(a) suggest that both the phase composition and the growth of crystals were sensitive to the calcination temperature. At 500°C and 600°C (not shown), no other phases were found except the phases of the starting ZnO (zincite), TiO_2 (anatase) and SnO_2 (cassiterite) components. A reaction between ZnO and TiO_2 to form

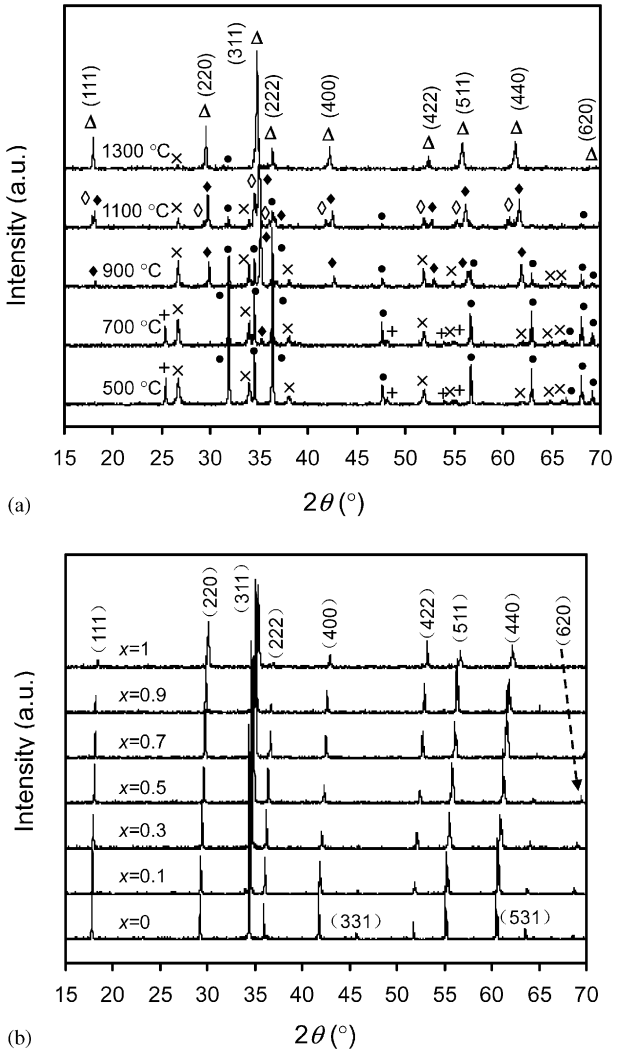

Fig. 1. (a) XRD patterns of the $ZnO/TiO_2/SnO_2$ mixture with a Zn/Ti/Sn molar ratio of 4:1:1 after calcination for 2 h at the indicated temperatures (+: anatase TiO_2; ×: SnO_2; •: ZnO; ◆: Zn_2TiO_4; ◇: Zn_2SnO_4; △: $Zn_2Ti_{0.5}Sn_{0.5}O_4$); (b) XRD patterns of the $Zn_2Ti_xSn_{1-x}O_4$ ($x = 0$, 0.1, 0.3, 0.5, 0.7, 0.9, 1) solid solutions obtained by calcination at 1300°C for 42 h.

Zn_2TiO_4 (JCPDS 77–0014) took place during the calcination at 700–900°C, consistent with the results in Refs. [6–9]. However, the X-ray diffraction patterns show no evidence for the formation of $ZnTiO_3$ and $Zn_2Ti_3O_8$, which is at variance with the results in Refs. [7–9]. The characteristic diffractions of anatase TiO_2 were hardly detectable after the calcination at 800°C for 2 h (not shown), and they disappeared completely after the calcination at 900°C for 2 h, suggesting that all the TiO_2 reacted or became amorphous or otherwise undetectable to the X-ray diffraction technique. The growth of Zn_2TiO_4 continued with increasing the calcination temperature up to 1000°C (not shown), when the calcined mixture were composed of ZnO, SnO_2 and Zn_2TiO_4 phases. Another new phase Zn_2SnO_4 (JCPDS 74–2184) appeared after the calcination at 1100°C for 2 h, which is consistent with the result in Ref. [24]. Thus, the phase components at 1100°C were Zn_2TiO_4, Zn_2SnO_4 and small amounts of residual ZnO (zincite) and SnO_2 (cassiterite). Further increasing the calcination temperature up to 1200°C caused both Zn_2TiO_4 and Zn_2SnO_4 phases to react to form a new phase with a set of diffractions at $2\theta = 18.00°$, 29.66°, 34.91°, 36.47°, 42.40°, 52.64°, 56.08°, 61.57°, which may be a solid solution $Zn_2Ti_xSn_{1-x}O_4$ ($0 < x < 1$). The formation and growth of the $Zn_2Ti_xSn_{1-x}O_4$ ($0 < x < 1$) solid solution continued when the temperature was further increased to 1300°C. Residual ZnO (zincite) and SnO_2 (cassiterite) almost disappeared at 1300°C, implying that the product can be approximately viewed as $Zn_2Ti_{0.5}Sn_{0.5}O_4$.

The XRD pattern of the solid solution $Zn_2Ti_{0.5}Sn_{0.5}O_4$ was indexed referencing to the Zn_2SnO_4 and Zn_2TiO_4 inverse spinels (Fig. 1(a)). It seems that the calcination for 2 h at 1300°C is not sufficient and should be extended to induce a complete transformation of the mixture into the solid solution $Zn_2Ti_{0.5}Sn_{0.5}O_4$, which with the diffractions at $2\theta = 18.04°$, 29.59°, 34.84°, 36.44°, 42.29°, 46.32°, 52.42°, 55.86°, 61.24°, 64.40°, 69.42°. In view of this, the calcination period was extended to 6, 10, 14, 18, 22, 26, 30, 34, 38 and 42 h at 1300°C, respectively, and it was found that a period of 42 h is enough for such a purpose (see Fig. 1(b)). Therefore, all the $ZnO/TiO_2/SnO_2$ mixtures were calcined at 1300°C for 42 h to prepare the solid solution $Zn_2Ti_xSn_{1-x}O_4$ materials (white in color). From Fig. 1(b), it can be seen that the XRD patterns of the product powders are very similar to each other except the regular shifts of XRD peaks towards somewhat higher angles with the increase of x in the composition. All the XRD patterns could be indexed (Fig. 1(b)) by assuming a face-centered cubic structure for the solid solution. Therefore, each of the materials shown in Fig. 1(b) can be taken as a single-phase solid solution with an inverse spinel-like structure (space group O_h^7-$Fd3m$), expressed as $Zn_2Ti_xSn_{1-x}O_4$ ($x = 0$, 0.1, 0.3, 0.5, 0.7, 0.9, 1). The unit cell of the $Zn_2Ti_xSn_{1-x}O_4$ materials should have 8 A_2BX_4 units (A=Zn, B=Ti and/or Sn, X=O) ($Z = 8$) that involve a total of 56 atoms [8,34]. In these inverse spinel structures the cations (Zn^{2+}, Ti^{4+} and Sn^{4+}) could be arranged as $Zn_{tetra}[ZnTi_xSn_{1-x}]_{octa}O_4$, i.e. one half of the Zn^{2+} ions are in the tetrahedral sites; the other half of the Zn^{2+} ions plus the Ti^{4+} and/or Sn^{4+} ions occupy the octahedral sites [8,34,35]. The cubic lattice constants (a) of the $Zn_2Ti_xSn_{1-x}O_4$ solid solutions, calculated with the software (Diffrac^{plus} Win-Metric Version 3.0) on the X-ray diffractometer, are 8.649, 8.631, 8.594, 8.547, 8.506, 8.477, and 8.440 Å, corresponding to $x = 0$, 0.1, 0.3, 0.5, 0.7, 0.9 and 1, respectively. The calculation error in the lattice constants is ± 0.003 Å. Fig. 2 shows the change of lattice constant of the solid solution $Zn_2Ti_xSn_{1-x}O_4$ ($0 \leqslant x \leqslant 1$) with composition. It can be seen that the lattice constant decreases linearly with the increasing Ti content, obeying approximately the generally known Vegard's law. This indicates that the lattice of the solid solution $Zn_2Ti_xSn_{1-x}O_4$ ($0 \leqslant x \leqslant 1$) evolves with composition from Zn_2SnO_4 to Zn_2TiO_4, due to the substitution of lattice Ti^{4+} with a smaller radius (0.68 Å) for the Sn^{4+} with a larger radius (0.71 Å). It should be noted that the lattice constants measured in the present work of the Zn_2SnO_4 ($x = 0$) and Zn_2TiO_4 ($x = 1$) are in good agreement with the standard values of 8.6500 Å for Zn_2SnO_4 (JCPDS 74–2184) and 8.4450 Å for Zn_2TiO_4 (JCPDS 77–0014). The cubic unit cell volumes of the $Zn_2Ti_xSn_{1-x}O_4$ ($0 \leqslant x \leqslant 1$) solid solutions were calculated to be 647.0, 643.0, 634.7, 624.4, 615.4, 609.2 and 601.2 Å^3 corresponding to $x = 0$, 0.1, 0.3, 0.5, 0.7, 0.9 and 1, respectively.

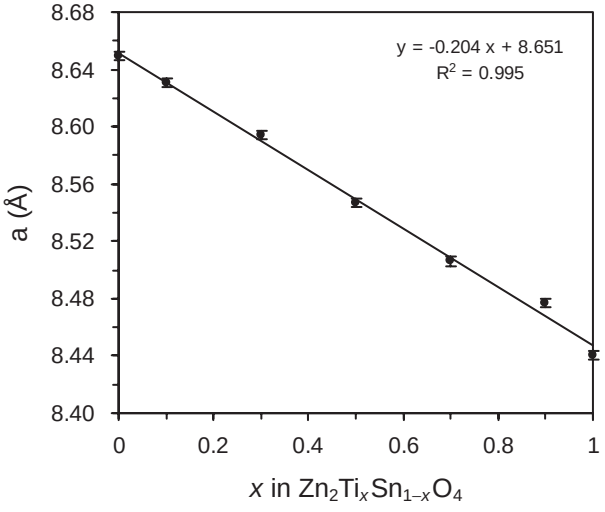

Fig. 2. Lattice constants of the $Zn_2Ti_xSn_{1-x}O_4$ ($x = 0$, 0.1, 0.3, 0.5, 0.7, 0.9, 1) solid solutions obtained by calcination at 1300°C for 42 h.

3.2. TG-DTA analysis

Fig. 3 shows the TG and DTA (heat flow) curves of the $ZnO/TiO_2/SnO_2$ mixture with a Zn/Ti/Sn molar ratio 4:1:1. The TG curve reveals no weight change of the sample in the temperature range 400–1400°C, while the endothermic effects at above 700°C is clearly seen on the DTA curve, and are further characterized by a strong endothermic peak at about 1190°C. The TG curve suggests no formation of volatile products. And, thus, the endothermic feature on the DTA curve must be associated with solid-state reactions and phase transformations in the mixed oxides at above 700°C. This explanation is consistent with the XRD results (Fig. 1(a)) that Zn_2TiO_4 and Zn_2SnO_4 were formed at about 700°C and 1100°C, respectively. In fact, the formations of Zn_2SnO_4 and Zn_2TiO_4 from ZnO and SnO_2, and ZnO and TiO_2, respectively, were found to be endothermic [12,36]. Therefore, the endothermic effects on the DTA curve in between 700°C and 1100°C should arise from the reactions leading to the formation of Zn_2TiO_4 and Zn_2SnO_4. Since all the materials reacted to form $Zn_2Ti_{0.5}Sn_{0.5}O_4$ solid solution at above 1200°C and the solid solution was found to be the only detectable product after the calcination at 1300°C, the strong endothermic peak at about 1190°C should be related with the formation of the $Zn_2Ti_{0.5}Sn_{0.5}O_4$ solid solution.

3.3. SEM/TEM Morphology and BET surface area

Fig. 4 shows the SEM and TEM micrograms of the $Zn_2Ti_{0.5}Sn_{0.5}O_4$ solid solution calcined at 1300°C for 42 h. The TEM micrograph show that the solid solution appears as irregular crystals of different sizes. The particles shown in the SEM micrograph also have irregular shapes. The average particle (SEM) and the crystal (TEM) sizes are estimated to be near 20 μm and 400 nm, respectively.

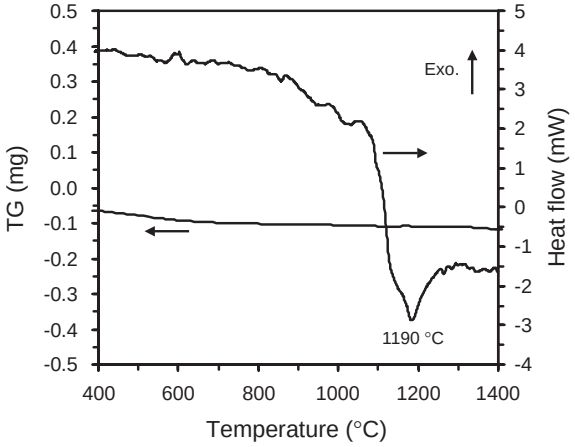

Fig. 3. TG-DTA curves of the $ZnO/TiO_2/SnO_2$ mixture with a molar ratio of 4:1:1 (starting sample weight: 44.33 mg; heating rate: 10°C/min).

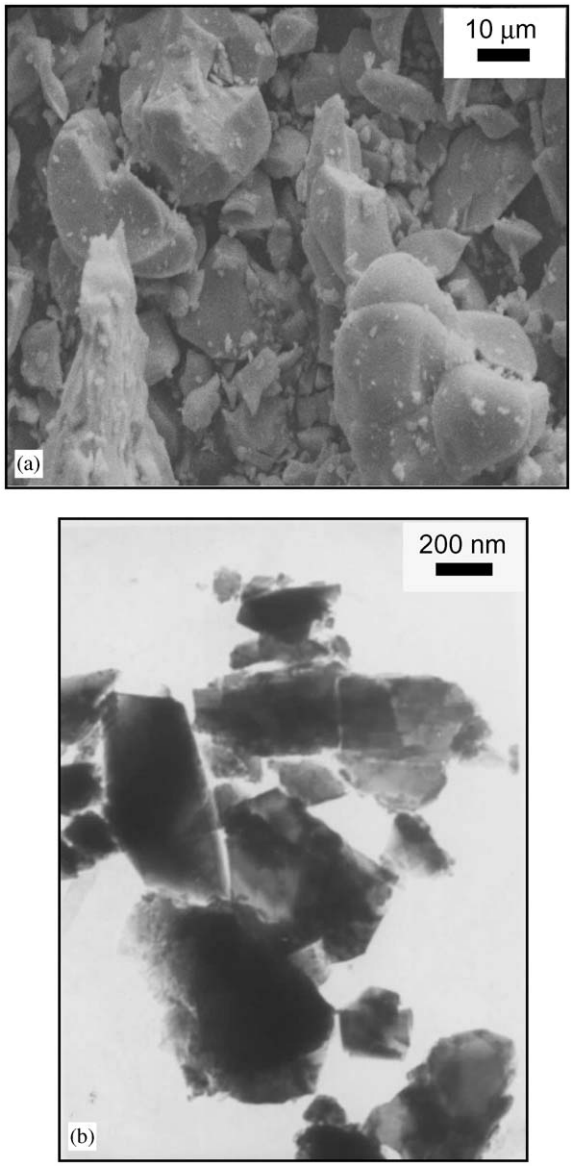

Fig. 4. (a) SEM and (b) TEM micrograms of the $Zn_2Ti_{0.5}Sn_{0.5}O_4$ solid solution calcined at 1300°C for 42 h.

The measured BET surface areas of the $Zn_2Ti_xSn_{1-x}O_4$ solid solutions shown in Fig. 1(b) are 0.22, 0.20, 0.19, 0.23, 0.21, 0.21 and 0.25 m^2/g for $x = 0$, 0.1, 0.3, 0.5, 0.7, 0.9 and 1, respectively. The small values in surface area seem to be in agreement with the big sizes of the samples, which are resulted from the high calcination temperature, as evidenced by Fig. 4(a).

3.4. Optical absorption property

Fig. 5 shows the UV–Vis diffuse reflectance spectra of the $Zn_2Ti_xSn_{1-x}O_4$ ($x = 0$, 0.1, 0.3, 0.5, 0.7, 0.9, 1) solid solutions calcined at 1300°C for 42 h. All these samples show optical absorption, similar to the Zn_2SnO_4 and

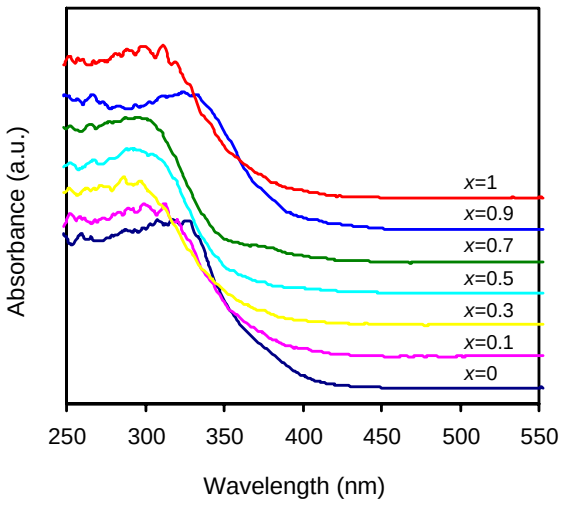

Fig. 5. UV–Vis diffuse reflectance spectra of the $Zn_2Ti_xSn_{1-x}O_4$ ($x = 0$, 0.1, 0.3, 0.5, 0.7, 0.9, 1) solid solutions calcined at 1300°C for 42 h.

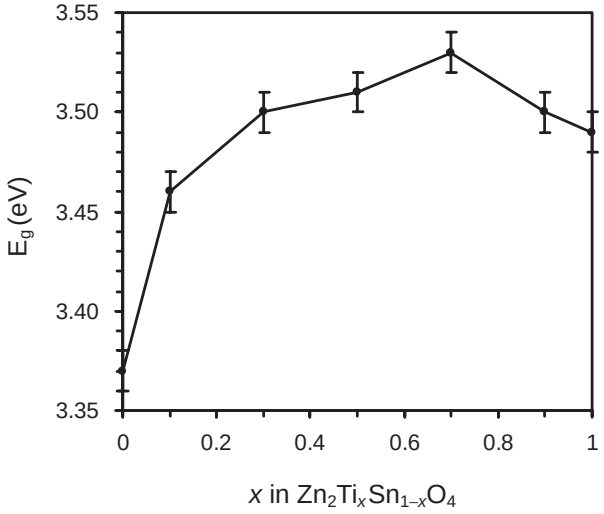

Fig. 6. Band gap energies of the $Zn_2Ti_xSn_{1-x}O_4$ ($x = 0$, 0.1, 0.3, 0.5, 0.7, 0.9, 1) solid solutions calcined at 1300°C for 42 h.

Zn_2TiO_4 reported by Enoki et al. [37] and Matsumoto et al. [38], respectively. The absorption edges were defined as the wavelengths at intersections that were obtained by extrapolating the horizontal and sharply rising portions of the UV–Vis absorption curves. The absorption edges of the $Zn_2Ti_xSn_{1-x}O_4$ solid solutions thus estimated are 368, 358, 353, 352, 351, 354 and 355 nm for the samples with $x = 0$, 0.1, 0.3, 0.5, 0.7, 0.9 and 1, respectively. Shown in Fig. 6 are the band gap energies (E_g) of the $Zn_2Ti_xSn_{1-x}O_4$ ($x = 0$, 0.1, 0.3, 0.5, 0.7, 0.9, 1) solid solutions, which were calculated from the corresponding data of the absorption edges [39]. The band gap energies of all the $Zn_2Ti_xSn_{1-x}O_4$ ($0 \leqslant x \leqslant 1$) solid solutions are larger than ZnO (3.2 eV) and TiO_2 (3.2 eV), but smaller than SnO_2 (3.6 eV) [39]. A maximum band gap energy ($E_g = 3.53$ eV) was found for the sample with $x = 0.7$. The band gap energies of these $Zn_2Ti_xSn_{1-x}O_4$ ($0 \leqslant x \leqslant 1$) solid solutions suggests that the materials belong to semiconductors and potential applications as electronic and gas-sensing materials could be expected. Generally, the band structure of metal oxides is defined by the *d* levels of the metal cations and the 2*p* level of the oxygen anions [40–44]. For the $Zn_2Ti_xSn_{1-x}O_4$ ($0 \leqslant x \leqslant 1$) solid solutions, the valence bands may be mainly composed of the O 2*p* orbits, which may be hybridized slightly with the Zn 3*d*, Sn 4*d* and/or Ti 3*d* orbits. On the other hand, the conduction bands may be mainly composed of the Zn 3*d*, Sn 4*d* and/or Ti 3*d* orbits in the tetrahedral ZnO_4 and octahedral $[ZnTi_xSn_{1-x}]O_6$ units [41–44]. In comparison with the Zn 3*d* and Sn 4*d* orbits, the Ti 3*d* orbits could contribute more significantly to the conduction band because they are not fully occupied and little localized, but the Zn 3*d* and Sn 4*d* orbits are fully occupied. Therefore, the band gap energies of the $Zn_2Ti_xSn_{1-x}O_4$ ($0 \leqslant x \leqslant 1$) solid solutions will change with the increasing Ti content, which is consistent with the experimental results.

4. Conclusions

Single-phase $Zn_2Ti_xSn_{1-x}O_4$ ($0 \leqslant x \leqslant 1$) solid solutions with an inverse spinel structure (*Fd*3*m*) can be synthesized by calcining the stoichiometric solid-mixtures of ZnO, TiO_2 and SnO_2 at 1300°C for 42 h. The $Zn_2Ti_xSn_{1-x}O_4$ ($0 \leqslant x \leqslant 1$) solid solutions show optical absorptions in the near ultraviolet region. The Ti content has a significant effect on the absorption edge and thus the band gap energy of the solid solution; the sample with $x = 0.7$ shows the maximum band gap energy ($E_g = 3.53$ eV). The $Zn_2Ti_xSn_{1-x}O_4$ ($0 \leqslant x \leqslant 1$) solid solutions are semiconductors and may find applications in the optoelectronic, gas-sensing and microwave dielectric fields.

Acknowledgments

The authors would like to thank Mr. Jingzhi Wei, Mr. Ruji Wang and Mr. Yu Wu for their helps in this work. This work was financially supported by NSF China (Grant: 20125310).

References

[1] H.P. Naidu, A.V. Virkar, J. Am. Ceram. Soc. 81 (1998) 2176–2180.
[2] F. Edelman, H. Hahn, S. Seifried, C. Alof, H. Hoche, A. Balogh, P. Werner, K. Zakrzewska, M. Radecka, P. Pasierb, A. Chack, V. Mikhelashvili, G. Eisenstein, Mater. Sci. Eng. B 69–70 (2000) 386–391.

[3] K. Vinodgopal, I. Bedja, P.V. Kamat, Chem. Mater. 8 (1996) 2180–2187.
[4] M.M. Oliveira, D.C. Schnitzler, A.J.G. Zarbin, Chem. Mater. 15 (2003) 1903–1909.
[5] I. Bedja, P.V. Kamat, J. Phys. Chem. 99 (1995) 9182–9188.
[6] N.W. Taylor, Z. Physik. Chem. B 9 (1930) 241–264.
[7] F.H. Dulin, D.E. Rase, J. Am. Ceram. Soc. 43 (1960) 125–131.
[8] S.F. Bartram, R.A. Slepetys, J. Am. Ceram. Soc. 44 (1961) 493–499.
[9] J. Yang, J.H. Swisher, Mater. Character. 37 (1996) 153–159.
[10] G. Marci, V. Augugliaro, M.J.L. Munoz, C. Martin, L. Palmisano, V. Rives, M. Schiavello, R.J.D. Tilley, A.M. Venezia, J. Phys. Chem. B 105 (2001) 1033–1040.
[11] N. Nikolic, T. Sreckovic, M.M. Ristic, J. Euro. Ceram. Soc. 21 (2001) 2071–2074.
[12] C. Wang, X.M. Wang, J.C. Zhao, B.X. Mai, G.Y. Sheng, P.A. Peng, J.M. Fu, J. Mater. Sci. 37 (2002) 2989–2996.
[13] C. Wang, J.C. Zhao, X.M. Wang, B.X. Mai, G.Y. Sheng, P.A. Peng, J.M. Fu, Appl. Catal. B: Environ. 39 (2002) 269–279.
[14] K. Tennakone, I.R.M. Kottegoda, L.A.A. De Silva, V.P.S. Perera, Semicond. Sci. Technol. 14 (1999) 975–978.
[15] K. Zakrzewska, Thin Solid Films 391 (2001) 229–238.
[16] L.B. Kong, J. Ma, H. Huang, J. Alloys Compd. 336 (2002) 315–319.
[17] J. Lin, J.C. Yu, D. Lo, S.K. Lam, J. Catal. 183 (1999) 368–372.
[18] M. Radecka, K. Zakrzewska, M. Rekas, Sensor. Actuator. B 47 (1998) 194–204.
[19] O. Yamaguchi, M. Morimi, H. Kawabata, K. Shimizu, J. Am. Ceram. Soc. 70 (1987) C-97–C-98.
[20] Y.S. Chang, Y.H. Chang, I.G. Chen, G.J. Chen, Y.L. Chai, J. Cryst. Growth 243 (2002) 319–326.
[21] H.T. Kim, S. Nahm, J.D. Byun, Y. Kim, J. Am. Ceram. Soc. 82 (1999) 3476–3480.
[22] H.T. Kim, J.D. Byun, Y. Kim, Mater. Res. Bull. 33 (1998) 963–973.
[23] Z.X. Chen, A. Derking, W. Koot, M.P. van Dijk, J. Catal. 161 (1996) 730–741.
[24] T. Hashemi, H.M. Al-allak, J. Illingsworth, A.W. Brinkman, J. Woods, J. Mater. Sci. Lett. 9 (1990) 776–778.
[25] J. Fang, A.H. Huang, P.X. Zhu, N.S. Xu, J.Q. Xie, J.S. Chi, S.H. Feng, R.R. Xu, M.M. Wu, Mater. Res. Bull. 36 (2001) 1391–1397.
[26] X.H. Wu, Y.D. Wang, Z.H. Tian, H.L. Liu, Z.L. Zhou, Y.F. Li, Solid-State Electron. 46 (2002) 715–719.
[27] D. Kovacheva, K. Petrov, Solid State Ionics 109 (1998) 327–332.
[28] J.D. Perkins, J.A. del Cueto, J.L. Alleman, C. Warmsingh, B.M. Keyes, L.M. Gedvilas, P.A. Parilla, B. To, D.W. Readey, D.S. Ginley, Thin Solid Films 411 (2002) 152–160.
[29] X.H. Wu, Y.D. Wang, H.L. Liu, Y.F. Li, Z.L. Zhou, Mater. Lett. 56 (2002) 732–736.
[30] Z.Y. Yuan, F. Huang, J.T. Sun, Y.H. Zhou, Chem. Lett. (2002) 408–409.
[31] T.J. Coutts, D.L. Young, X. Li, W.P. Mulligan, X. Wu, J. Vac. Sci. Technol. A 18 (2000) 2646–2660.
[32] F. Belliard, P.A. Connor, J.T.S. Irvine, Solid State Ionics 135 (2000) 163–167.
[33] J.H. Yu, G.M. Choi, Sensor. Actuactor. B 72 (2001) 141–148.
[34] W.B. White, B.A. Deangelis, Spectrochim. Acta 23A (1967) 985–995.
[35] E.J.W. Verwey, E.L. Heimann, J. Chem. Phys. 15 (1947) 174–180.
[36] M. Ocana, W.P. Hsu, E. Matijevic, Langmuir 7 (1991) 2911–2916.
[37] H. Enoki, T. Nakayama, J. Echigoya, Phys. Stat. Sol. (a) 129 (1992) 181–191.
[38] Y. Matsumoto, M. Omae, I. Watanabe, E. Sato, J. Electrochem. Soc. 133 (1986) 711–716.
[39] A. Hagfeldt, M. Grätzel, Chem. Rev. 95 (1995) 49–68.
[40] M. Yoshino, M. Kakihana, W.S. Cho, H. Kato, A. Kudo, Chem. Mater. 14 (2002) 3369–3376.
[41] D.E. Scaife, Solar Energy 25 (1980) 41–54.
[42] Z.G. Zou, J.H. Ye, H. Arakawa, J. Phys. Chem. B 106 (2002) 517–520.
[43] D.W. Hwang, J.S. Lee, W. Li, S.H. Oh, J. Phys. Chem. B 107 (2003) 4963–4970.
[44] J. Yin, Z.G. Zou, J.H. Ye, J. Phys. Chem. B 107 (2003) 61–65.